A Three-Winding Common Mode Inductor

Chi Kwan Lee, *Senior Member, IEEE*, Danting Xu, *Student Member, IEEE*,
Bryan M. H. Pong, *Senior Member, IEEE*, Sitthisak Kiratipongvoot, and Wai Man Ng, *Member, IEEE*

***Abstract*—Electronic products consist of parasitic capacitance between the circuit components and the ground, which introduces common mode (CM) noise. A CM inductor is used to block the noise following into the power supply affecting the others. However, the CM inductor and the parasitic capacitance could create resonance phenomenon that affect the filter performance in low frequency. In this paper, we investigate into this resonance phenomenon by giving a detailed analysis of the CM inductor and filter configuration. A three-winding CM inductor is then proposed to solve the aforementioned problem. This three-winding CM inductor consists of two traditional CM inductor winding and an auxiliary winding connecting to a negative impedance converter. The impedance of the CM inductor is virtually boosted up. Without physically increasing the value of the inductance, the noise attenuation in low frequency is improved and the resonance phenomenon is significantly mitigated. A prototype is constructed and practically tested on a 100-W switched-mode power supply. Experimental results show that the three-winding CM inductor operates as theoretically anticipated. The noise level at the resonant frequency is reduced by 21 dB, whereas the power consumption of the additional circuit only consumes 0.5 W.**

***Index Terms*—Common mode (CM) inductor, electromagnetic interference (EMI), negative impedance converter (NIC).**

I. Introduction

SWITCHED-MODE power supplies (SMPS) use pulse width modulation in response to the supply's operation and load's condition. The high-frequency edges of the rectangular waveforms contain high frequency harmonics which are the root cause of the electromagnetic interference (EMI). High emission of EMI could seriously affect the neighbor electronic system in normal operation. Therefore, SMPSs are required to comply with electromagnetic compatibility (EMC) tests [1]–[3]. Usually SMPSs could pass the radiated EMI tests because the magnetic field does not reach very far. However, conducted EMI propagating along the power line could cause interference to other electronic equipments. Conducted EMI is classified into two modes: the differential mode (DM) and common mode (CM) [3]. CM noise is more difficult to handle than DM noise because the noise comes from the capacitive coupling between the noise source and the power lines [4]. The noise path is invisible, as a result, numerous techniques such as filtering, shielding [5], and design optimization [6]–[8] are developed to tackle the CM noise problems.

Passive EMI filters in *LC* and *LCL* configurations are the most popular solutions, as they are low cost and very reliable. However, the inductors and capacitors could be large and bulky for filtering low-frequency switching noise. The design of passive EMI filter needs to carefully consider the parasitic inductance and capacitance of the components which could create low-frequency resonance deteriorating the filter performance [9], [10]. To substantially reduce the size and weight of the filter, active EMI filtering techniques are proposed to meet the increasing demand for highly compact product design [11]–[14]. In general, active EMI filter uses the current or voltage cancelation techniques to remove the low-frequency noise. The circuit consists of a sensor, an injector, and an active control circuit [15]–[17]. In [18], an active CM inductor is proposed. The CM inductor is separated into two inductors connected in series. One is designated as sensor, the other as the injector. The current sensor and voltage injector require coupling transformers, which lead to increase the cost and power loss [19], [20]. The voltage sensor and current injector mostly employ coupling capacitors, the sizes of which are limited by the maximum leakage current to ground [21]. To achieve noise current or voltage cancellation, active EMI filter uses feedback or feed-forward control methods. Using the feedback control method, design engineer only takes into account the disturbance at the ac mains and does not need the details of the noise source [21], [22]. This method needs a high gain operational amplifier and proper tuning of the circuit. Feed-forward control method does not need high gain amplifier, but it requires high accuracy of amplifier gain control [20], [21]. The hybrid EMI filters in [23]–[25] combine a passive and an active EMI filter. While the active EMI filter is designed to attenuate the low-frequency noise, the corner frequency of the passive filter is placed after the active filter. Thus, the inductance and capacitance of the passive filter can be reduced. The overall size and weight of the filter are significantly trimmed down. The benefits of using active EMI filter are well proven, but the design complexity and cost need to be justified in the application.

In this paper, we present a three-winding CM inductor [26] which consists of a small and simple operational amplifier circuit called a negative impedance converter (NIC) [27], [28]. The impedance of the three-winding CM inductor is virtually increased several times comparing with the traditional CM inductor with the same number of turns. The original windings and ferrite core are remained unchanged. The auxiliary winding and the operational amplifier circuit are inherently isolated

Manuscript received July 28, 2016; accepted August 30, 2016. Date of publication September 14, 2016; date of current version February 27, 2017. The work was supported by a grant from the General Research Fund sponsored by the Research Grants Council of Hong Kong (17211515). Recommended for publication by J. M. Rivas Davila.

The authors are with the Department of Electrical and Electronic Engineering, The University of Hong Kong, Pok Fu Lam, Hong Kong (e-mail: cklee@eee.hku.hk; xudt@hku.hk; mhp@eee.hku.hk; ksitthis@eee.hku.hk; wmng@eee.hku.hk).

Color versions of one or more of the figures in this paper are available online at http://ieeexplore.ieee.org.

Digital Object Identifier 10.1109/TPEL.2016.2609435

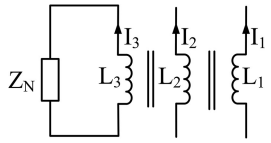

Fig. 1. Schematic of the three-winding CM inductor.

from the ac mains. This paper is organized as follows. The principle of the three-winding CM inductor is introduced in Section II. The insertion loss analysis of CM filter is provided in Section III. The design of a NIC to realize virtual impedance boosting is explicated in Section IV. The experiment results to validate the proposed technique are presented in Section V. Section VI is the conclusion of the paper.

II. Operating Principle of the Three-Winding CM Inductor

A. Coupling Model

Fig. 1 depicts the schematic of the three-winding CM inductor. It consists of two CM windings for the power paths (i.e., Live and Neutral wires) and one auxiliary winding for connecting to an auxiliary impedance Z_N. All the windings are wound on the same magnetic core. L_1 and L_2 denote the CM windings while L_3 denotes the auxiliary winding. The equivalent impedance of the windings in general form are expressed as

$$\begin{aligned} Z_1 &= \frac{V_1}{I_1} = sL_1 + sM_{21}\frac{I_2}{I_1} + sM_{31}\frac{I_3}{I_1} \\ Z_2 &= \frac{V_2}{I_2} = sM_{12}\frac{I_1}{I_2} + sL_2 + sM_{32}\frac{I_3}{I_2} \\ Z_3 &= \frac{V_3}{I_3} = sM_{13}\frac{I_1}{I_3} + sM_{23}\frac{I_2}{I_3} + sL_3 \end{aligned} \tag{1}$$

where Z_1, Z_2, and Z_3 are equivalent impedance of windings L_1, L_2, and L_3, respectively. I_i and V_i are the corresponding CM noise current and voltage of L_i where i = 1, 2, 3. $M_{\rm ij}$ $(i, j = 1, 2, 3$ and $i \neq j)$ are the mutual inductance between the windings. Applying general assumption, the windings are made to be identical (i.e., $L_i = L_{\rm CM}$). Only CM currents are considered. I_1 and I_2 are theoretically the same, so $I_1 = I_2 = I$.

For simplicity, the mutual inductance between the windings are assumed to be the same (i.e., $M_{\rm ij} = M$). It is because the windings are wound on the same magnetic core and considered well coupled together. Simplifying (1), the CM impedance $Z_{\rm CML}$ can be written as

$$Z_{\rm CML} = Z_1 = Z_2 = s(L_{\rm CM} + M) + Z_{\rm AUX} \tag{2}$$

where $s(L_{\rm CM} + M)$ is the original equivalent impedance of the CM windings in power paths. The auxiliary impedance is $Z_{\rm AUX} = -\frac{2\times s^2 M^2}{Z_N + sL_{\rm CM}}$ which can be used to reshape the frequency response of the CM inductor.

B. Auxiliary Impedance

In [7] and [26], a series resistor–inductor (RL) network was chosen as the Z_N to mitigate the low-frequency resonance between the CM inductor and the parasitic capacitance of the converter. However, this proposal reduces the inductance of the CM inductor, as a result diminishing the high-frequency performance of the EMI filter. It can be observed from (2) that $Z_{\rm AUX}$ is a negative term while Z_N is positive. Thus, $Z_{\rm CML}$ will always be smaller than the original impedance $s(L_{\rm CM} + M)$, if Z_N is a passive network. The effectiveness of the EMI noise attenuation will be diminished. In order to solve this problem, we propose using a negative inductor to virtually boost up the CM impedance. The impedance characteristic of a negative inductor $(L_N < 0)$ is similar to an ordinary inductor except that its voltage is lagging behind the current by 90°. Mathematically, when $Z_N = -s|L_N|$, the equivalent impedance of $Z_{\rm CML}$ becomes

$$Z_{\rm CML} = s(L_{\rm CM} + M) + s\frac{2M^2}{|L_N| - L_{\rm CM}}. \tag{3}$$

L_N could affect the CM impedance of the CM inductor in the following three cases:

1) $|L_N| > L_{\rm CM}$: $Z_{\rm AUX}$ is positive, $Z_{\rm CML}$ increases;
2) $|L_N| < L_{\rm CM}$: $Z_{\rm AUX}$ is negative, $Z_{\rm CML}$ decreases;
3) $|L_N| = L_{\rm CM}$: $Z_{\rm AUX}$ is infinite, $Z_{\rm CML}$ becomes infinite.

A technical term to describe the boost of the CM impedance of the three-winding CM inductor is defined as

$$A_{\rm CML} = \frac{Z_{\rm CML}}{s(L_{\rm CM} + M)}. \tag{4}$$

Solving (3) and (4), we obtain the value of the negative inductor L_N directly as

$$L_N = -\frac{2M^2}{(A_{\rm CML} - 1)(L_{\rm CM} + M)} - L_{\rm CM}. \tag{5}$$

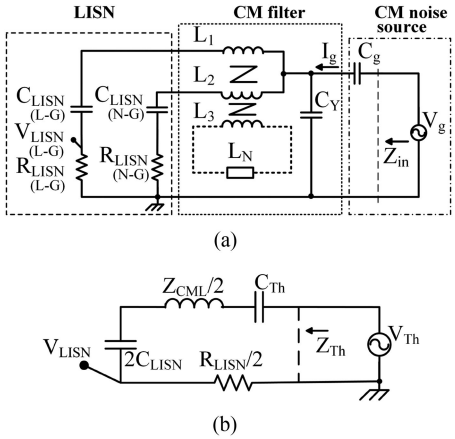

Fig. 2. (a) CM noise model and (b) its Thevinin's equivalent circuit.

III. CM Noise Model and Analysis

Based on a practical SMPS, a CM noise model is built to investigate the characteristics of the CM filter. This CM noise model consists of a noise source, CM filter, and line impedance stabilization network (LISN) as shown in Fig. 2(a). The CM noise source denoted as V_g and C_g represents the total parasitic capacitance between the converter and the ground. C_g exists when the components are proximity to the grounded chassis. An example of C_g is the parasitic capacitance between the power

TABLE I
COMPONENTS VALUES OF THE CM NOISE MODEL

LISN		CM filter	
C_{LISN}	0.1 μF	L_{CM}	2.1 mH
R_{LISN}	50 Ω	M	2.1 mH
C_g	94 pF	C_Y	2 nF
L_N (Three-winding CM inductor only)			-3 mH
V_g (Square wave)			2 V at 25 kHz

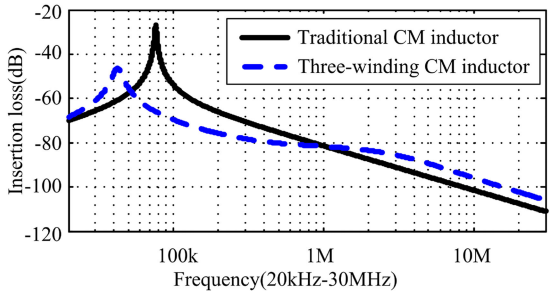

Fig. 3. Insertion loss calculation of the CM filters using traditional and the three-winding CM inductors.

device and heat sink. L_{CM} and C_Y represent the self-inductance and Y-capacitance of the CM filter, respectively. The LISN is also modeled as a series resistor–capacitor (*RC*) network. The detailed parameters are summarized in Table I.

To analytically obtain the insertion loss of the CM filter, we simplify the model using Thevinin's theorem. The simplified CM noise model is shown in Fig. 2(b). $C_{\mathrm{Th}} = C_Y + C_g$ is Thevinin's equivalent capacitance and $V_{\mathrm{Th}} = (C_g/C_{\mathrm{Th}})V_g$ is the equivalent voltage source. Z_{Th} is the input impedance. Thus, the insertion loss $|I_{\mathrm{L}}|_{\mathrm{dB}}$ of the CM filter can be written as

$$|I_{\mathrm{L}}|_{\mathrm{dB}} = 20\log_{10}\left(\frac{C_g}{C_{\mathrm{Th}}} \times \frac{R_{\mathrm{LISN}}}{2|Z_{\mathrm{Th}}|}\right) \tag{6}$$

and Z_{Th} can be expressed as

$$Z_{\mathrm{Th}} = \frac{1}{sC_{\mathrm{Th}}} + \frac{R_{\mathrm{LISN}}}{2} + \frac{1}{s \times 2C_{\mathrm{LISN}}} + \frac{Z_{\mathrm{CML}}}{2} \tag{7}$$

where

$$Z_{\mathrm{CML}} = \begin{cases} s(L_{\mathrm{CM}} + M) & \text{Traditional} \\ s(L_{\mathrm{CM}} + M) + \frac{2sM^2}{|L_N| - L_{\mathrm{CM}}}. & \text{Three-winding.} \end{cases} \tag{8}$$

Fig. 3 plots the insertion loss of the CM filter with different configurations. It can be observed that the traditional CM inductor combined with the parasitic capacitance and Y-capacitors create a low-frequency resonance at 77 kHz. While typical SMPS usually operate from tens to hundred kilohertz, the noise suppression performance of the CM filter in the low-frequency band is diminished. Conversely, the three-winding CM inductor performs well by boosting the CM impedance and shifting the resonant frequency to 41 kHz. The insertion loss of the CM filter from the frequency of 50–800 kHz has significantly improved.

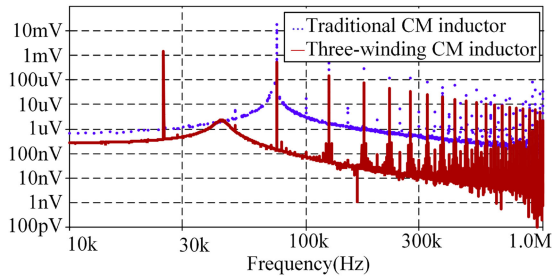

Fig. 4. Simulated noise spectra of the EMI filter using traditional and the three-winding CM inductors.

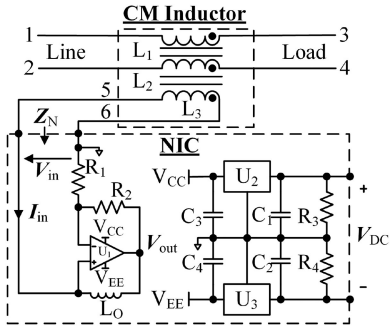

Fig. 5. Schematic of the NIC and its connection diagram.

It can be expected that the CM filter with the three-winding CM inductor could provide better noise attenuation in the low frequency than using the traditional CM inductor.

In order to evaluate the noise attenuation of the traditional and the three-winding CM inductors, The CM noise model as shown in Fig 2 (a) is put into the PSpice simulator. The negative inductor L_N is created by a NIC. The noise source V_g is replaced by a square wave running at 25 kHz. The spectrum of the noise voltage V_{LISN} is measured at the resistor $R_{\mathrm{LISN(L-G)}}$. In Fig. 4, the fundamental frequency of two CM filters are similar. The noise level using the three-winding CM inductor at the fundamental frequency is 1.4573 $\mathrm{mV_{pk}}$ (63.27 dBμV). On the other hand, using traditional CM filter is 1.1161 $\mathrm{mV_{pk}}$ (61 dBμV). The noise level is only slightly increased by 0.3412 mV (2.27 dB). Note that there is a significant improvement at the third harmonic (i.e., 75 kHz) using the three-winding CM filter so it achieves additional 31 dB suppression. The third harmonic using traditional CM filter is 18.158 mV (85.4 dBμV). The three-winding CM filter reduces the third harmonic down to 525.3 μV (54.4 dBμV).

IV. DESIGN AND IMPLEMENTATION OF THE NIC

A. Circuit Analysis

A negative inductor can be created by a NIC, which is a one-port Op-Amp circuit sensing the voltage at its input and inject a current I_{in} from its output to the input side through an inductor L_O (see Fig. 5). This topology is also called as current-inversion NIC. In contrast to the ordinary Op-Amp circuits, NIC employs both negative and positive feedback connections. The connections of the NIC and the three-winding CM inductor are also shown in Fig. 5.

TABLE II
COMPONENTS VALUES OF THE NIC CIRCUIT

U_1	LF353	R_1	1.125 kΩ
U_2	LM78L12ACM	R_2	1 kΩ
U_3	LM79L12ACM	R_3, R_4	10 kΩ
C_1, C_2	10 μF	L_O	2.7 mH, 60 mA
C_3, C_4	1 μF		

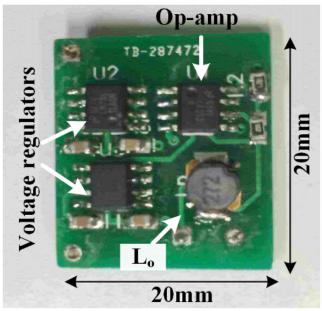

Fig. 6. Photo of the NIC.

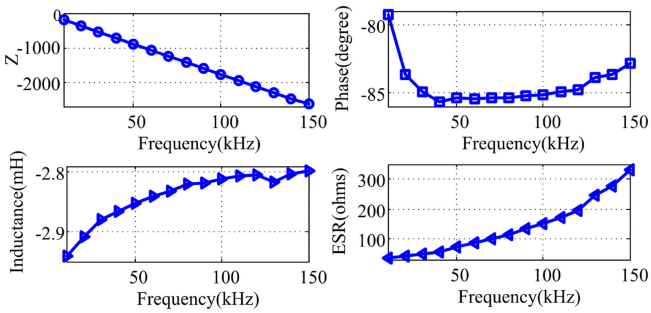

Fig. 7. Measured impedance, phase angle, equivalent inductance, and ESR of the NIC.

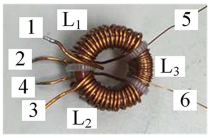

Fig. 8. Photo of the three-winding CM inductor.

The analysis of the NIC is shown here. The output voltage and current can be expressed as

$$\begin{cases} \mathbf{V}_{\text{out}} = \left(1 + \frac{R_2}{R_1}\right) \mathbf{V}_{\text{in}} \\ \mathbf{I}_{\text{in}} = \frac{\mathbf{V}_{\text{in}} - \mathbf{V}_{\text{out}}}{\mathbf{Z}_{L_o}} \end{cases} \tag{9}$$

where R_2 and R_1 are the resistors of the negative feedback circuit. $\mathbf{V}_{\text{out}}$ is the output voltage (in vector form) of the Op-Amp. $\mathbf{V}_{\text{in}}$ and $\mathbf{I}_{\text{in}}$ are the input voltage and current of the NIC, respectively. $\mathbf{Z}_{L_o}$ is the impedance of the inductor L_o. The ratio of $\frac{R_1}{R_2}$ determines the close-loop gain of the NIC. Dividing $\mathbf{V}_{\text{in}}$ with $\mathbf{I}_{\text{in}}$, it gives the equivalent impedance of the NIC as

$$\mathbf{Z}_N = \frac{\mathbf{V}_{\text{in}}}{\mathbf{I}_{\text{in}}} = -\frac{R_1}{R_2}\mathbf{Z}_{L_o} \approx -\frac{R_1}{R_2} s L_O. \tag{10}$$

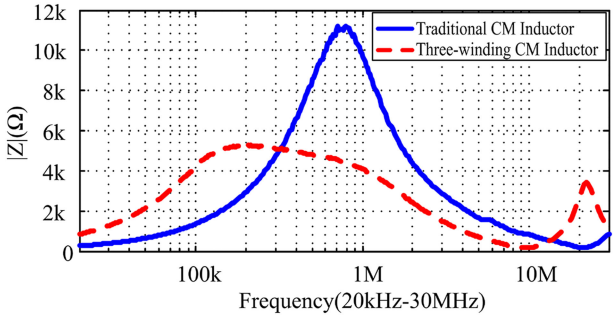

Fig. 9. CM impedance of the traditional and the three-winding CM inductors.

B. Design and Implementation

The design of NIC should meet some important criteria in order to ensure the circuit functioning properly.

1) The bias current (i.e., $I_{\text{B}+}$) of the Op-Amp should be small. Thus, the input current of the NIC is almost equal to the current of the inductor L_O. The current phase angle of the NIC is approximately equal to 90° with the input voltage.
2) The current in the negative feedback (i.e., I_{f}) circuit should be small. The output current of the Op-Amp is almost equal to the current of the inductor L_O. Thus, the power of the NIC can be reduced.
3) The dc gain of the Op-Amp should be close to unity (typical 1–2). Since the performance of an Op-Amp is limited by the gain bandwidth product, this helps to improve the frequency response of the Op-Amp as a result maximizing the bandwidth of the NIC.
4) The resistance of the inductor L_O should be kept small, even though L_O does not carry high current. The resistance of L_O increases the ESR of L_N. Equation (3) shows that the boosting of the CM impedance comes from the $(|L_N| - L_{\text{CM}})$.

To validate the proposed method, a CM inductor is chosen for the modification. The original inductance of the CM inductor is 2.1 mH. The expected boosting coefficient (A_{CML}) of CM impedance is 3.33. Using (5) and (10) the values of the negative inductor L_N and the output inductor of the NIC are calculated as -3 and 2.7 mH, respectively. To meet the aforementioned criteria, a JFET input operational amplifier LF353 is used. The gain bandwidth product is as high as 4 MHz and the input bias current is as low as 50 pA. A linear power supply module is built for the NIC. It converts an external 48 V_{dc} source into a $\pm 12\ \text{V}_{\text{dc}}$ source for the Op-Amp. In the practical implementation, the external 48 V_{dc} source is not required. Power could come from the output or internal auxiliary supply of the power converter. A list of the components and their parameters are summarized in TABLE II. All the components are in surface mounted device package and built on a 20 mm × 20 mm printed circuit board as shown in Fig. 6.

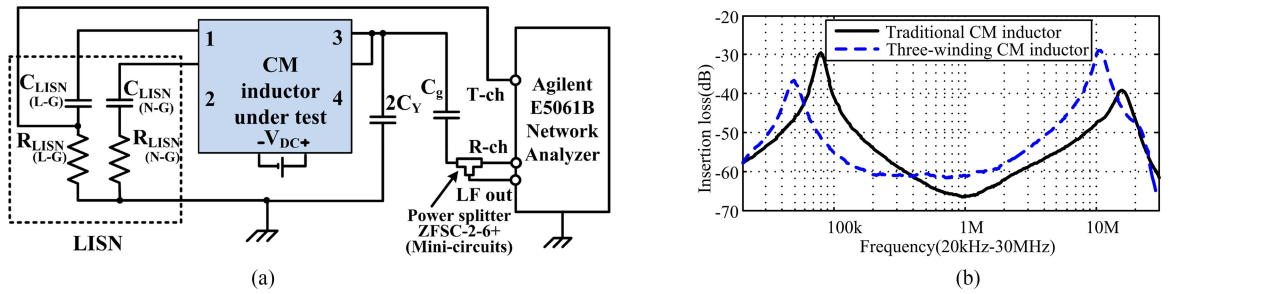

Fig. 10. Configuration and insertion loss measurement of the CM filters using traditional and the three-winding CM inductors. (a) Configuration for the insertion loss measurement. (b) Insertion loss measurement results.

Fig. 11. Photo of the practical implementation: (a) SMPS for practical implementation. (b) Installation of the purposed CM inductor.

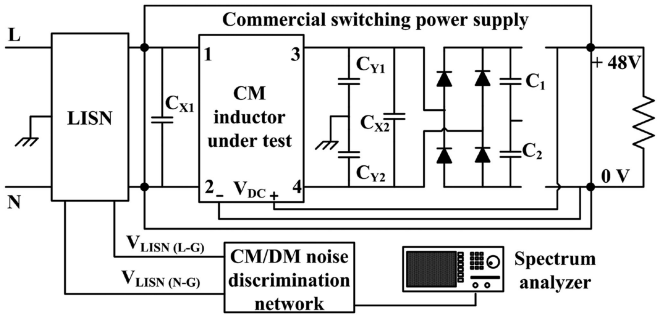

Fig. 12. Configuration for the conducted EMI test.

C. Inductance Measurement

Since the characteristic of the NIC is different from an ordinary inductor, a method is formulated to measure the impedance and phase angle of the NIC. First, a network impedance analyzer is used to measure the impedance and phase angle of the inductor L_O at different frequencies (i.e., from 10 to 150 kHz). Second, the NIC is connected to a sinusoidal wave generator. The phase angle between the input $\mathbf{V}_{\rm in}$ and output $\mathbf{V}_{\rm out}$ voltage of the operational amplifier operating at different frequencies is measured using an oscilloscope. Using (9) and (10), the impedance of the NIC can be obtained.

Fig. 7 shows the measured results of the NIC including the impedance, equivalent inductance, phase, and equivalent series resistance (ESR). It is important to note that the impedance of the NIC increases when the frequency increases. The negative sign of the impedance indicates the phase angle is negative, in which the input voltage $\mathbf{V}_{\rm in}$ lags behind the input current $\mathbf{I}_{\rm in}$. The equivalent inductance of the NIC is measured between -2.8 and -2.9 mH which is closely equal to the theoretical expected value -3 mH. The phase angle and ESR are also examined to verify the operation of the circuit.

V. Practical Implementation of the Three-Winding CM Inductor

Fig. 8 shows the photo of the three-winding CM inductor. The numbers denote the connection terminals according to the schematic as shown in Fig. 5. Auxiliary winding L_3 only carries CM noise current which is very small. The winding is wound with thin wire. The size of the core is as same as the traditional CM inductor. The CM impedance is measured by an Agilent E5061B impedance analyzer and plotted in Fig. 9. The CM impedance of the three-winding CM inductor is increased in the low frequency (i.e., <300 kHz) compared with the traditional CM inductor. It is anticipated that the CM filter using the three-winding CM inductor can obtain a lower resonant frequency and provide a higher insertion loss in the low frequency than using the traditional CM inductor.

A. Insertion Loss Measurement

The test setup for the insertion loss measurement using an Agilent E5061B network analyzer is shown in Fig. 10(a). The configuration is based on the CM noise model as shown in Fig. 2(a). To facilitate the measurement, a two-way power splitter is used to provide the reference signal for the R-ch from the source. The R-ch receiver monitors the source output voltage V_g applied to the CM filter. The T-ch receiver monitors the voltage at the $R_{\rm LISN}$. Then, the analyzer measures the voltage ratio $V_{\rm RLISN}/V_g$ which indicates the insertion loss of the

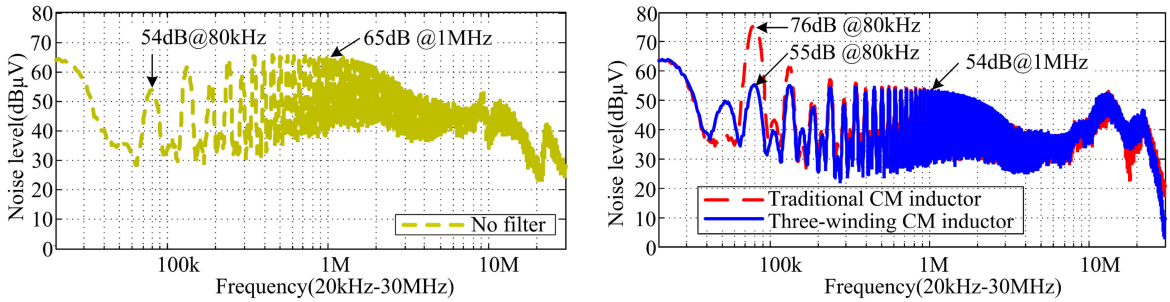

Fig. 13. CM noise spectrum of the SMPS (a) without EMI filter and (b) with different EMI filter configurations.

CM filter. The measurement results of the traditional and the three-winding CM inductors are shown in Fig. 10(b). The measurement results are consistent with the theoretical expectation in which the three-winding CM inductor could have a higher insertion loss in the low frequency. With the use of proposed NIC connected across the auxiliary winding, the CM impedance is increased and the resonance is shifted from 80 to 48 kHz. Over -15 dB of attenuation can be observed at 100 kHz which is the range of high-frequency noise generated by modern SMPS. The high-frequency resonance of the CM inductor due to the winding capacitance stays in the similar place. It is slightly shifted from 17 to 11 MHz. It is important to note that frequencies from 50 kHz to 10 MHz are the typical range of frequencies of interest for ac mains conducted EMI. Above 10 MHz, the effect of the board's layout becomes dominant and noise could become radiated interference.

B. Practical Implementation

The three-winding CM inductor is practically implemented in a 100-W commercial SMPS [see Fig. 11(a)] to demonstrate the effectiveness of the proposal. The switching frequency of the SMPS is 22 kHz. The input and output voltages are 220 V_{ac} and 48 V_{dc}, respectively. The proposed three-winding CM inductor can directly replace the traditional CM inductor because they occupy a similar footprint area, as shown in Fig. 11(b). The NIC circuit board is installed next to the CM inductor. The parameters of the EMI filter and NIC can be referred to Tables I and II. A pair of dc supply wire provides a 48 V_{dc} supply from the SMPS output to the NIC circuit board. Fig. 11(b) shows the details of the modifications work. The measurement of conducted EMI is carried in a shielded room. The noise spectra of the power supply at full load with and without EMI filters are measured.

Fig. 12 depicts the setup for conducted EMI measurement. The SMPS is connected to the ac mains through the LISN. The LISN represents the standardized impedance of the power network. The noise signals of the line and neutral conductors are taken from this impedance with a high-pass filter. $V_{\mathrm{LISN(L-G)}}$ and $V_{\mathrm{LISN(N-G)}}$ denote the noise signal on line and neutral conductor which contain both CM and DM noise. A CM/DM noise discrimination network is used to extract CM noise. The CM noise level is measured by Agilent CXA N9000A Signal Analyzer.

C. Results and Comparison

After removing the EMI filter from the SMPS, the noise spectrum is recorded as shown in Fig. 13(a). Without EMI filter, the CM noise level between 200 kHz and 2 MHz is about 65 dB. In the second experiment, the EMI filter using a traditional CM inductor is installed. In Fig. 13(b), the red curve shows the CM noise spectrum of EMI filter using a traditional CM inductor. It can be observed that 10 dB attenuation is achieved around 1 MHz. However, the low-frequency resonance can also be observed at 80 kHz. Thus, the noise level at resonant frequency significantly increases from 54 to 76 dB. The noise attenuation is also weak when the noise frequency is close to the resonant frequency. For instance, noise level at 130 kHz is similar to no filter applied. In the third experiment, the traditional CM inductor is replaced by the three-winding CM inductor. In Fig. 13(b), the blue curve shows the noise spectrum of EMI filter using the three-winding CM inductor. The measurement result shows that the three-winding CM inductor provides good noise attenuation from 80 kHz to 2 MHz. The noise level is below 55 dB. As a comparison, 21 dB attenuation is achieved at the resonant frequency (i.e., 80 kHz). The new resonant frequency is relocated at 50 kHz which is very close to the theoretical analysis. In the high frequency (i.e., >1 MHz), the performance of the three-winding CM inductor is as good as the traditional CM inductor. The efficiency of the SMPS is measured by PM100 power analyzer at full load condition. Using traditional and the three-winding CM inductors, efficiency of 89.7% and 89.4% is measured. There is no significant increase in power loss. The power consumption of NIC is found to be 0.5 W.

VI. Conclusion

Based on the coupling model of a three-winding CM inductor, a general form of the equivalent CM impedance is derived. The mathematical expression shows that the impedance connected across the third winding can reshape the frequency response of the CM inductor. While a negative inductor is connected, the CM impedance is virtually boosted up. This technique is very useful to attenuate the low-frequency switching noise from 50 to 500 kHz. The design of the NIC together with the practical implementation on a commercial 100-W SMPS is described in detail. The NIC is very small, very robust, low cost, and requires no tuning. The additional circuit can be easily fitted into exist-

ing SMPS without major modifications. Experimental results show that the three-winding CM inductor overcomes the problem of the low-frequency resonance in the CM filter, whereas the high-frequency noise attenuation remains the same as the traditional CM inductor. The measured power consumption of the additional circuit is only 0.5 W which is not significant to the overall system efficiency.

REFERENCES

[1] G. L. Skibinski, R. J. Kerkman, and D. Schlegel, "EMI emissions of modern PWM AC drives," *IEEE Ind. Appl. Mag.*, vol. 5, no. 6, pp. 47–80, Nov./Dec. 1999.

[2] K. Mainali and R. Oruganti, "Conducted EMI mitigation techniques for switch-mode power converters: A survey," *IEEE Trans. Power Electron.*, vol. 25, no. 9, pp. 2344–2356, Sep. 2010.

[3] T. Guo, D. Y. Chen, and F. C. Lee, "Separation of the common-mode- and differential-mode-conducted EMI noise," *IEEE Trans. Power Electron.*, vol. 11, no. 3, pp. 480–488, May 1996.

[4] R. L. Ozenbaugh and T. M. Pullen, *EMI Filter Design*, 3rd ed. Boca Raton, FL, USA: CRC Press, Sep. 2011.

[5] L. Xie, X. Ruan, Q. Ji, and Z. Ye, "Shielding-cancelation technique for suppressing common-mode EMI in isolated power converters," *IEEE Trans. Ind. Electron.*, vol. 62, no. 5, pp. 2814–2822, May 2015.

[6] M. Pahlevaninezhad, D. Hamza, and P. K. Jain, "An improved layout strategy for common-mode EMI suppression applicable to high-frequency planar transformers in high-power dc/dc converters used for electric vehicles," *IEEE Trans. Power Electron.*, vol. 29, no. 3, pp. 1211–1228, Mar. 2014.

[7] P. Wang, F. Zheng, Y. Zhang, J. Wang, and X. Yang, "EMI filter optimization by adjusting common mode noise impedance of a balanced boost converter," in *Proc. 2013 IEEE ECCE Asia Downunder*, Jun. 2013, pp. 872–876.

[8] P. Wang, "Research on EMI filter based on S-parameters," M.S. thesis, Xidian Univ., Xi'an, China, 2012.

[9] S. Wang and F. C. Lee, "Analysis and applications of parasitic capacitance cancellation techniques for EMI suppression," *IEEE Trans. Ind. Electron.*, vol. 57, no. 9, pp. 3109–3117, Sep. 2010.

[10] S. Wang, F. C. Lee, D. Y. Chen, and W. G. Odendaal, "Effects of parasitic parameters on EMI filter performance," *IEEE Trans. Power Electron.*, vol. 19, no. 3, pp. 869–877, May 2004.

[11] Y. Maillet, R. Lai, S. Wang, F. Wang, R. Burgos, and D. Boroyevich, "High-density EMI filter design for DC-fed motor drives," *IEEE Trans. Power Electron.*, vol. 25, no. 5, pp. 1163–1172, May 2010.

[12] M. Ali, E. Labour, F. Costa, and B. Revol, "Design of a hybrid integrated EMC filter for a DC–DC power converter," *IEEE Trans. Power Electron.*, vol. 27, no. 11, pp. 4380–4390, Nov. 2012.

[13] J. Biela, A. Wirthmueller, R. Waespe, M. L. Heldwein, K. Raggl, and J. W. Kolar, "Passive and active hybrid integrated EMI filters," *IEEE Trans. Power Electron.*, vol. 24, no. 5, pp. 1340–1349, May 2009.

[14] Y. Chu, S. Wang, and Q. Wang, "Modeling and stability analysis of active/hybrid common-mode EMI filters for DC/DC power converters," *IEEE Trans. Power Electron.*, vol. 31, no. 9, pp. 6254–6263, Sep. 2016.

[15] N. K. Poon, J. C. P. Liu, C. K. Tse, and M. H. Pong, "Techniques for input ripple current cancellation: Classification and implementation [in SMPS]," *IEEE Trans. Power Electron.*, vol. 15, no. 6, pp. 1144–1152, Nov. 2000.

[16] W. Chen, W. Zhang, X. Yang, Z. Sheng, and Z. Wang, "An experimental study of common- and differential-mode active EMI filter compensation characteristics," *IEEE Trans. Electromagn. Compat*, vol. 51, no. 3, pp. 683–691, Aug. 2009.

[17] M. L. Heldwein, H. Ertl, J. Biela, and J. W. Kolar, "Implementation of a transformerless common-mode active filter for offline converter systems," *IEEE Trans. Ind. Electron.*, vol. 57, no. 5, pp. 1772–1786, May 2010.

[18] P. C. Murphy, T. C. Neugebauer, C. Brasca, and D. J. Perreault, "An active ripple filtering technique for improving common-mode inductor performance," *IEEE Power Electron Lett.*, vol. 2, no. 2, pp. 45–50, Jun. 2004.

[19] D. Hamza, M. Sawan, and P. K. Jain, "Suppression of common-mode input electromagnetic interference noise in DC-DC converters using the active filtering method," *IET Power Electron.*, vol. 4, pp. 776–784, Aug. 2011.

[20] S. Wang, Y. Y. Maillet, F. Wang, D. Boroyevich, and R. Burgos, "Investigation of hybrid EMI filters for common-mode EMI suppression in a motor drive system," *IEEE Trans. Power Electron.*, vol. 25, no. 4, pp. 1034–1045, Apr. 2010.

[21] W. Chen, X. Yang, and Z. Wang, "A novel hybrid common-mode EMI filter with active impedance multiplication," *IEEE Trans. Ind. Electron.*, vol. 58, no. 5, pp. 1826–1834, May 2011.

[22] W. Chen, X. Yang, J. Xue, and F. Wang, "A novel filter topology with active motor CM impedance regulator in PWM ASD system," *IEEE Trans. Ind. Electron.*, vol. 61, no. 12, pp. 6938–6946, Dec. 2014.

[23] W. C. Ho, C. K. Lee, X. Liu, P. K. W. Chan, S. Y. R. Hui, and Y. S. Lee, "A hybrid EMI filter with ultra-wide bandwidth," in *Proc. 2008 IEEE Appl. Power Electron. Conf. Expo.*, Feb. 2008, pp. 676–681.

[24] M. Zhu, D. J. Perreault, V. Caliskan, T. C. Neugebauer, S. Guttowskiand, and J. G. Kassakian, "Design and evaluation of feedforward active ripple filters," *IEEE Trans. Power Electron.*, vol. 20, no. 2, pp. 276–285, Mar. 2005.

[25] A. C. Chow and D. J. Perreault, "Design and evaluation of a hybrid passive/active ripple filter with voltage injection," *IEEE Trans. Aerosp. Electron. Syst.*, vol. 39, no. 2, pp. 471–480, Apr. 2003.

[26] D. Xu, W. M. Ng, S. Kiratipongvoot, C. K. Lee, and B. M. H. Pong, "A tunable common mode inductor with an auxiliary winding network," in *Proc. 2015 IEEE Appl. Power Electron. Conf. Expo.*, Mar. 2015, pp. 170–176.

[27] W. Li, R. Chen, N. Zhai, S. Li, and R. Mittra, "Wideband matching of an electrically small antenna using a negative impedance converter technique," in *Proc. 2012 IEEE Int. Symp. Antennas Propag. Soc.*, Jul. 2012, pp. 1–2.

[28] Y. Shen and T. H. Chio, "Limitation of negative impedance converter using operational amplifier for matching electrically small antenna," in *Proc. 2013 IEEE Int. Symp. Antennas Propag. Soc.*, Jul. 2013, pp. 1962–1963.

Chi Kwan Lee (M'08–SM'14) received the B.Eng. and Ph.D. degrees in electronic engineering from the City University of Hong Kong, Kowloon, Hong Kong, in 1999 and 2004, respectively.

He is currently an Assistant Professor in the Department of Electrical and Electronic Engineering, The University of Hong Kong. From 2008 to 2011, he was a Lecturer of electrical engineering with the Hong Kong Polytechnic University, Hung Hom, Hong Kong. Since 2010, he has been a Visiting Researcher with Imperial College London, England, U.K. In 2006, he joined as a Research Fellow in the Centre of Power Electronics, City University of Hong Kong. He was a Postdoctoral Research Fellow in the Power and Energy Research Centre, National University of Ireland, Galway, Ireland, from 2004 to 2005. His current research interests include wireless power transfer, clean energy technologies, and smart grids.

Dr. Lee received the IEEE POWER ELECTRONICS TRANSACTIONS First Prize Paper Award for his publications on Mid-Range Wireless Power Transfer in 2015. He is a co-inventor of the Electric Springs and planar EMI filter.

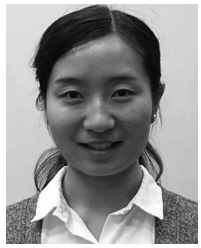

Danting Xu (S'16) received the B.Eng. degree in communication engineering from Xidian University, Xi'an, China, in 2011, and the M.Sc. degree in electrical & electronic engineering from The University of Hong Kong, Hong Kong, in 2012, where she is currently working toward the Ph.D. degree in power electronics.

Her current research interests include EMI reduction techniques and wireless power transfer.

Bryan M. H. Pong (M'4–SM'6) was born in Hong Kong. He received the B.Sc. degree in electronic and electrical engineering from the University of Birmingham, Birmingham, U.K., in 1983 and the Ph.D. degree in power electronics from Cambridge University, Cambridge, U.K., in 1987.

He worked with National Semiconductor Hong as a Chief Design Engineer. He also worked with ASTEC International as a Principal Engineer and a Division Engineering Manager. He is currently an Associate Professor with the University of Hong Kong, Hong Kong. He also holds a number of patents. His research interests include high efficiency and high reliability power conversion, EMI reduction techniques, magnetic components, bendable power converter, and other aspects of switch mode power conversion.

Sitthisak Kiratipongvoot received the B.Eng. and M.Eng. degrees in electrical engineering from King Mongkut's University of Technology North Bangkok, Bangkok, Thailand, in 2001 and 2008, respectively.

Since August 2012, he has been a Research Assistant in the Department of Electrical and Electronic Engineering, The University of Hong Kong, Hong Kong. His research interests include Resonant converters, EMI filter, and wireless energy transfer.

Wai Man Ng (M'04) received the B.Eng. (Hons.) and M.Phil. degrees from the City University of Hong Kong, Kowloon, Hong Kong, in 1998 and 2004, respectively, and the Ph.D. degree in power electronics from the University of Hong Kong, Pok Fu Lam, Hong Kong, in 2015.

From 1998 to 2000, he was an Electronic Engineer in the Astec Custom Limited. From 2000 to 2003, he was an Application Engineer in Ericsson Limited. From 2005 to 2011, he was a Research Fellow at the City University of Hong Kong. Since 2011, he has been with Department of Electrical and Electronic Engineering, University of Hong Kong, as a Research Officer. He is author or coauthor of more than 20 journals and conference papers. He holds three patents. His current research interests include application of power electronic in power system, electromagnetic interference, lighting technology, wireless power transfer, smart grid, and renewable energy application.